Supporting Information

Hydroxyl radical assisted enzyme-free electrochemical detection and oxidation of cholesterol by galvanically deposited layer-by-layer ZnO/WO₃ thin film nanocomposite

Uday Kumar Ghorui[†], Bibhutosh Adhikary[†*] and Anup Mondal[†*]

[†]*Department of Chemistry, Indian Institute of Engineering Science and Technology, Shibpur, Howrah 711 103, West Bengal, India*

Corresponding Authors

[*]E-mail: bibhutoshadhikary@gmail.com
[*]E-mail: anupmondal2000@yahoo.co.in

Materials and Chemicals

All the chemicals and materials were purchased of analytical grade and without further purification. Mili-Q water was used for all experiments unless mentioned otherwise. FTO glass substrate, Zn foil, disodium tungstate dihydrate ($Na_2WO_4, 2H_2O$), cholesterol, glucose, dopamine and β-estradiol were purchased from Sigma-Aldrich. Disodium hydrogen orthophosphate (Na_2HPO_4), ascorbic acid, uric acid, urea and hydroquinone were purchased from Merck Specialties Private Limited, India. Hydrochloric acid (HCl), nitric acid (HNO_3), phosphoric acid (H_3PO_4) and methanol (CH_3OH) were purchased from Spectrochem Pvt. Ltd.

Physical characterizations

X-ray diffraction of the films were performed with an X'Pert PRO parallel beam X-ray diffractometer using Bragg-Brentano focusing geometry and monochromatic CuKα radiation (λ = 1.540598 Å). Rietveld refinements were calculated using Full-Prof program in X'Pert PRO system. Thickness measurement of the samples were carried out with a Bruker Dektak XT stylus profilometer. Raman spectra were obtained on a Micro-Raman spectroscopy system RM 2000 (Renishaw in Via-reflex, 785 nm excitation laser). The surface morphology and the cross-sectional thickness of the synthesized thin films were examined under a field emission gun scanning electron microscopy (FEGSEM) (JEOL-JSM-7600F). Hitachi S-3400 N (EDX, Horiba EMAX) instrument was used to study energy dispersion X-ray spectroscopy (EDX). X-ray photoelectron spectra (Perkin-Elmer Physical Electronics 5600 spectrometer) were recorded to identify the chemical states of surface atoms and to confirm the existence of ZnO and WO_3 on FTO substrate. The electronic absorption spectra were investigated with a Carry-60, Agilent Technologies UV-Vis spectrophotometer. The photoluminescence (PL) spectra and lifetime

measurements were carried out with a Horiba Scientific Fluorolog instrument. All the electrochemical measurements were accomplished on a CHI660E Electrochemical Workstation.
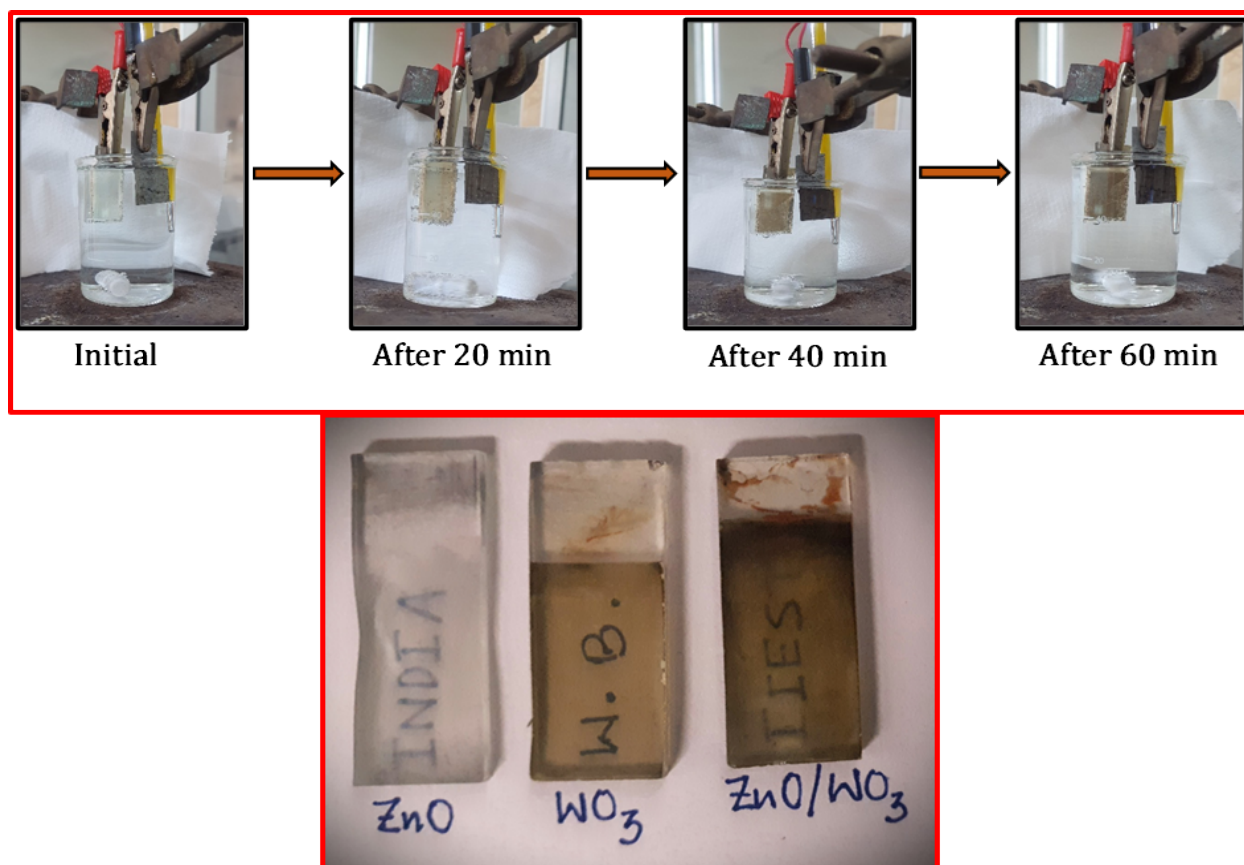

Fig. S1: Pictorial representation of development of WO_3 film on ZnO film using FTO substrate.
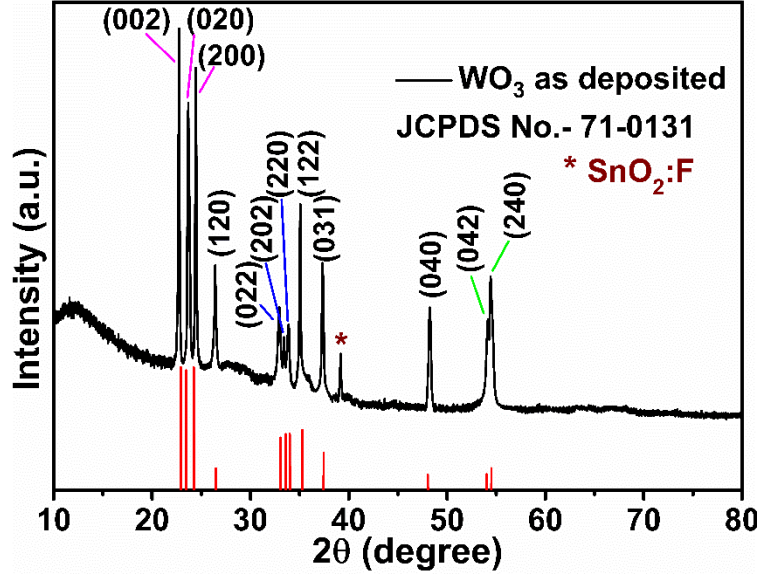
Fig. S2: X-ray diffraction patterns of as-deposited orthorhombic WO_3 thin film and pure WO_3.

Rietveld analysis of the films: To get a better conception of the structural parameters of thin films, Rietveld refined XRD analysis has been used, as shown in Fig. 1(a)-(c) (main manuscript). The Full-Prof program was applied to define XRD plane profile. The Rietveld refinement was implemented in X'Pert PRO system to calculate lattice constant (a, c), c/a ratio, unit cell volume (V), degree of distortion (R), interplanar distance (d) and bond length (along c axis) and have been presented in Table S1. The following equations were used to obtain the various data:

Degree of distortion: $R = \dfrac{2a\sqrt{2/3}}{c}$;   Volume: $V = \dfrac{\sqrt{3}}{2}a^3c$;

Interplanar distance: $\dfrac{1}{d^2} = \dfrac{4}{3}\left[\dfrac{h^2+hk+k^2}{a^2}\right] + \dfrac{l^2}{c^2}$;

Bond length of M-O: $L_{M\text{-}O} = \sqrt{\dfrac{a^2}{3} + (0.5 - u)^2 \times c^2}$; $u = \dfrac{a^2}{3c^2} + 0.25$;

The values of the structural parameters, as listed in Table S1 clearly depict that our synthesized thin film semiconductors are highly crystalline. The observed and calculated values matched well

with previous literature data.[1-3] The lattice parameters given in Table S1 (a and c) for the refined XRD patterns demonstrate a slight decrease for the composite film. This may be due to defects (such as vacancies, dislocation or interstitial), difference between the ionic radii of Zn^{2+} (0.74 Å) and W^{6+} (0.60 Å) or external strains grown because of temperature, etc.[2] It is evident that the c/a ratio remains almost same for all the films, but the distortion factor (R) increases slightly when WO_3 was deposited over ZnO film. This indicates that there must be some sort of distortion occurring in the crystal lattice.[4,5] Along with the lattice parameters (a and c), the unit cell volumes (V) and the crystallite sizes (D) of both ZnO and WO_3 films decreased progressively as the composite thin film gradually developed. The probable justification of the perceived trend is that there must be lattice contraction when the heterostructure grew. We have also noticed that the M-O bond lengths decreased from 1.981 to 1.977 Å for ZnO and 4.238 to 4.236 Å for WO_3 in ZnO/WO_3. Like the M-O bond length, the interplanar distance of the most intense peaks also decreased. This can be attributed to the higher electronegativity of W (2.36) as compared to Zn (1.65). The difference in electronegativity causes an increase in the attractive force between Zn and O atoms with respect to the force between W and O atoms.[5] Therefore, our synthesized annealed films match well with the structures of ZnO, WO_3 and ZnO/WO_3.

Table S1: Rietveld refinement of PXRD parameters of ZnO, WO_3 and ZnO/WO_3 thin films.

Samples	(hkl)	2θ (degree)	D (nm)	Lattice constant		c/a	R	V (Å³)	L_{M-O} (Å)	d (Å)
				a (Å)	c (Å)					
ZnO	(101)	36.46	144.2	3.250	5.208	1.602	1.018	47.64	1.981	2.478
WO₃	(200)	23.32	94.6	7.307	7.630	1.044	1.544	352.7	4.238	3.302
ZnO/WO₃	$(101)_{ZnO}$	36.22	109.0	3.248	5.206	1.603	1.021	47.56	1.977	2.475
	$(200)_{WO3}$	23.37	132.6	7.304	7.624	1.044	1.561	352.2	4.236	3.293

(a)

Elements	Weight %	Atomic %
O K	32.34	49.6
Zn L	67.66	50.4
Total	100	

(b)

Elements	Weight %	Atomic %
O K	37.46	75.3
W M	63.54	24.7
Total	100	

(c)

Elements	Weight %	Atomic %
O K	31.44	65.1
Zn L	23.39	16.6
W M	45.17	18.3
Total	100	
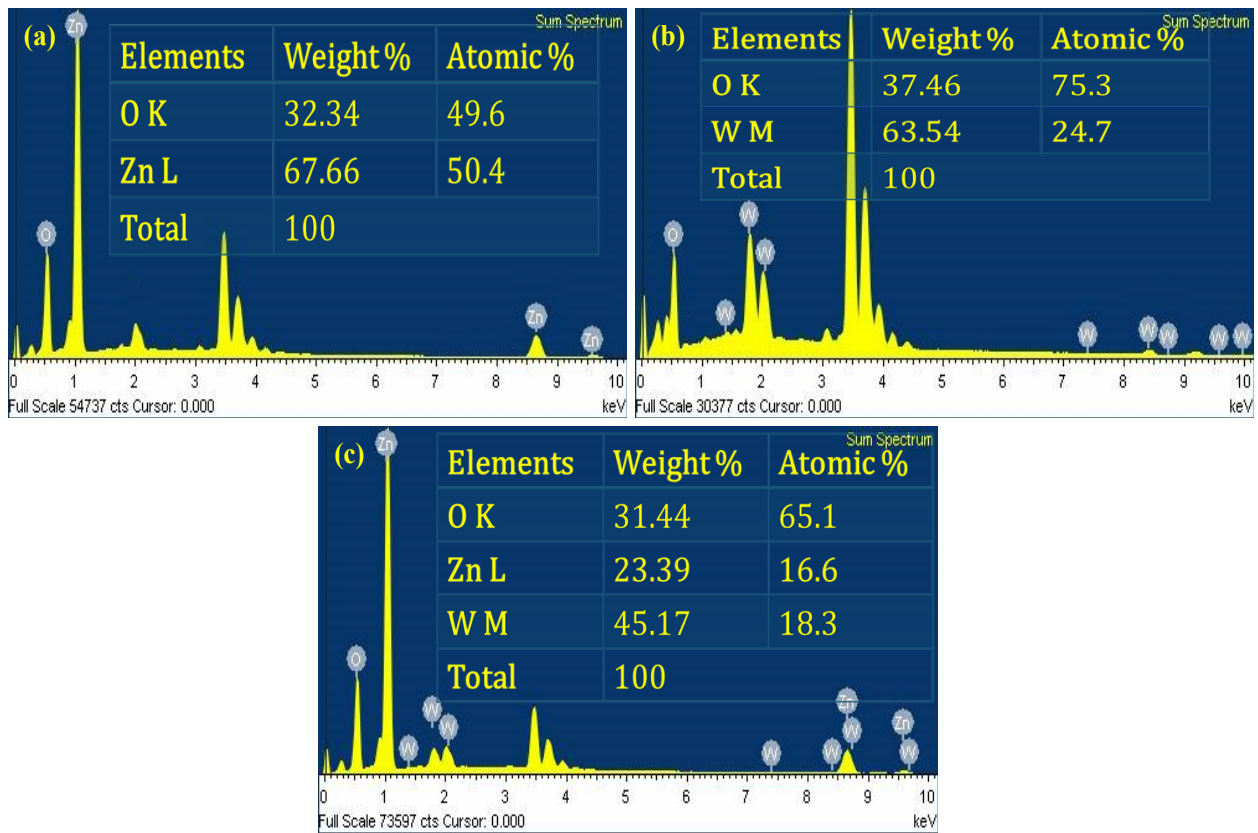
Fig. S3: (a), (b) and (c) are EDS spectra and corresponding EDS results of ZnO, WO$_3$ and ZnO/WO$_3$ thin films, respectively.
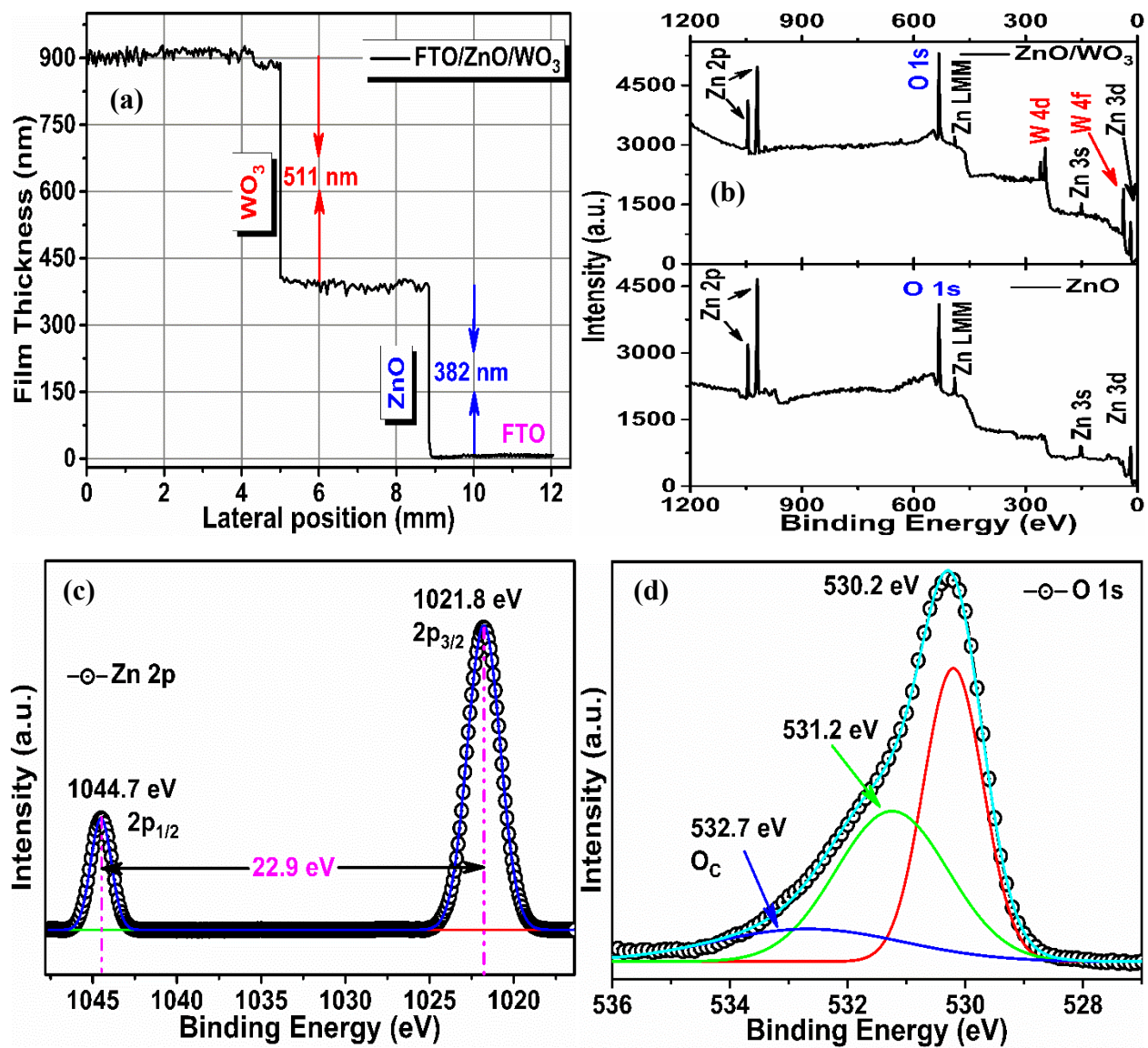
Fig. S4: (a) Thickness measurement of Layer-by-layer deposited ZnO/WO$_3$ on FTO by Stylus profilometry, (b) Survey scan of XPS for ZnO and ZnO/WO$_3$ thin films, (c) and (d) deconvoluted high resolution Zn 2p and O 1s peaks of ZnO film, respectively.
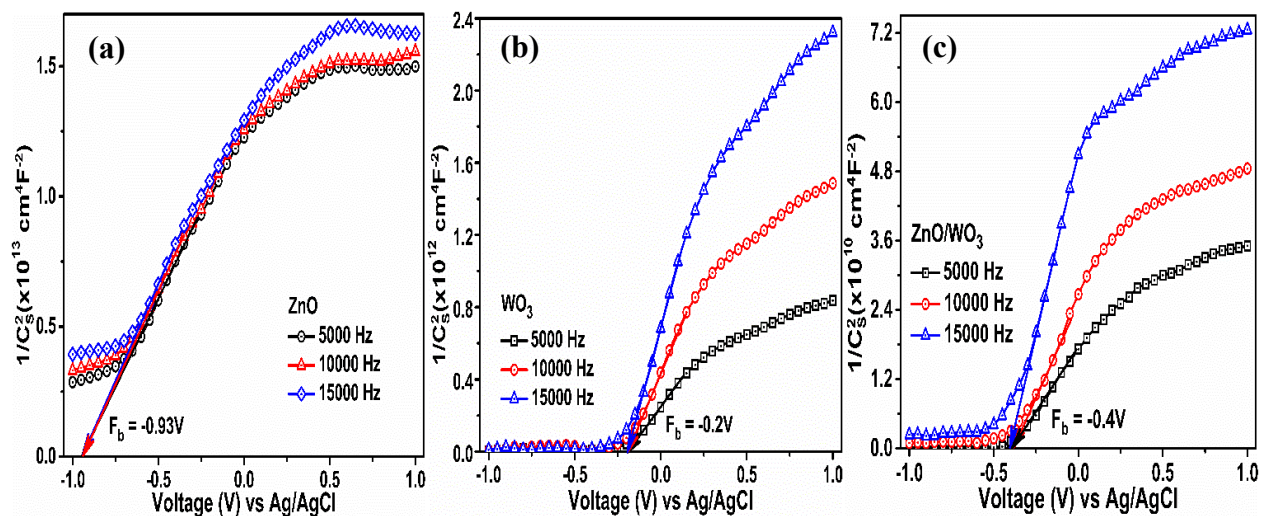
Fig. S5: Electrochemical Impedance-potential (Mott-Schottky) analyses of (a) ZnO, (b) WO$_3$ and (c) ZnO/WO$_3$ thin films.
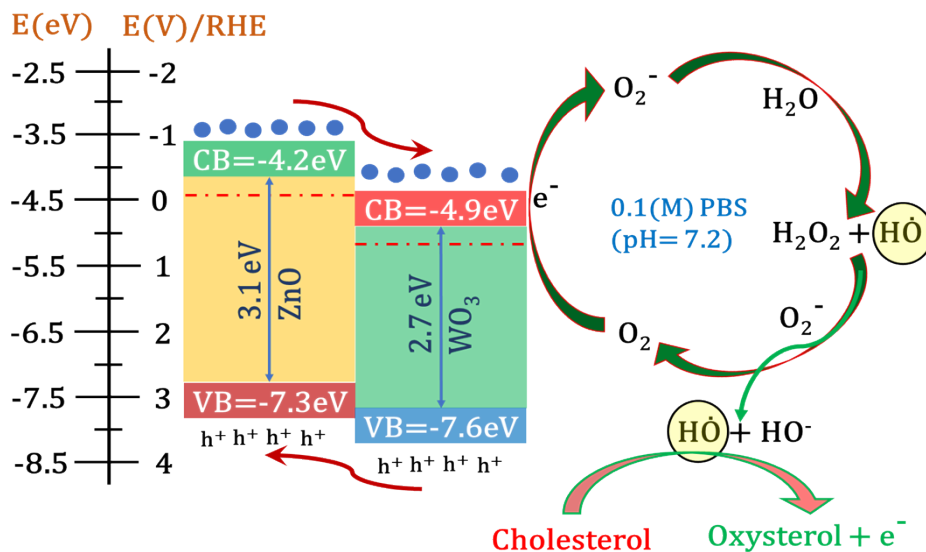

Fig. S6: Schematic representation of band energy diagram of ZnO/WO$_3$ heterostructure thin film for the electro-oxidation of ChOH.
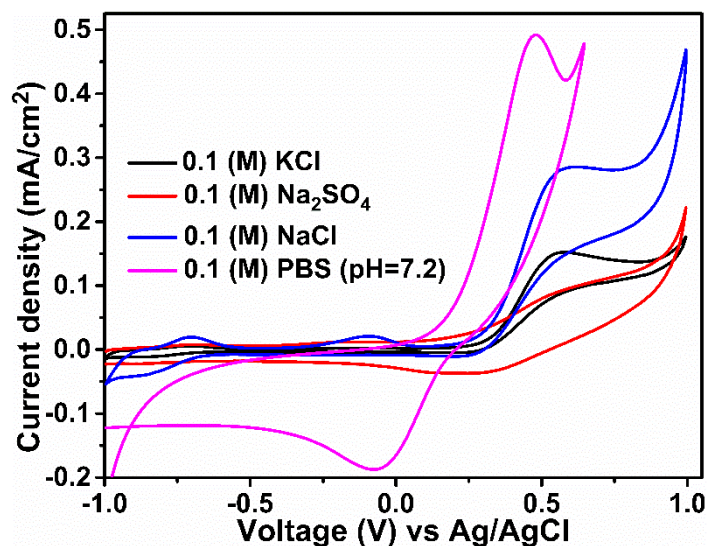
Fig. S7: CV profiles of ZnO/WO$_3$ composite thin films in different electrolytic solutions in presence of 30 μM ChOH at a scan rate of 50 mV/S.
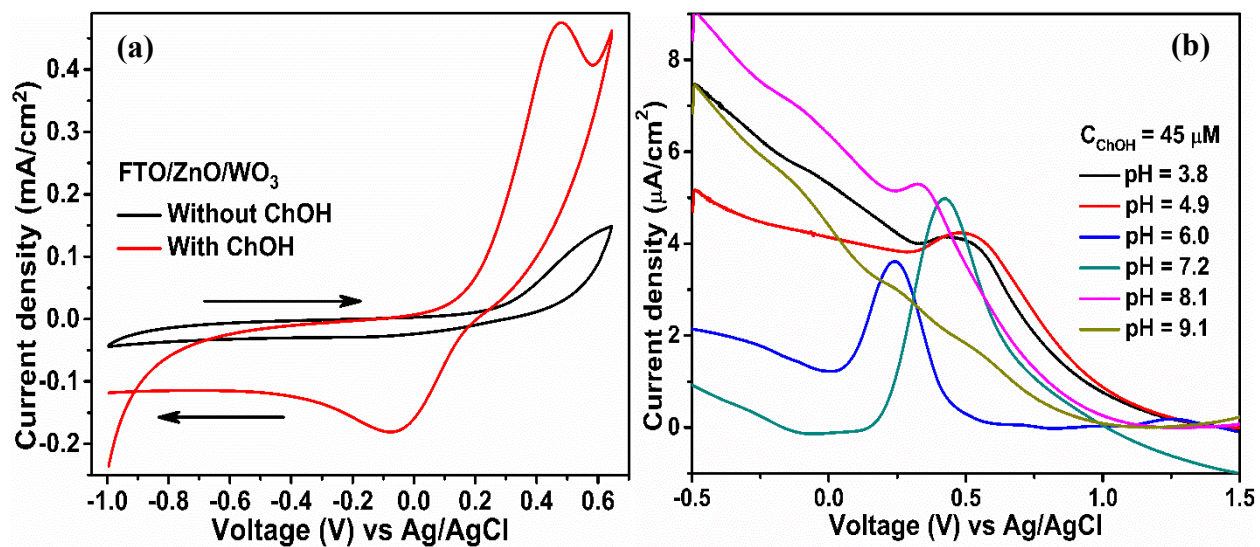

Fig. S8: (a) CV profiles of ZnO/WO$_3$ composite thin film in absence and presence of 30 μM ChOH in PBS at 50 mV/S scan rate; (b) DPV of ZnO/WO$_3$ thin film at different pH in presence of 45 μM ChOH in PBS.

Calculation of electron transfer kinetics:

The electrochemical activities of our thin film sensor are mostly represented by electron transfer rate constant (K_s) and electron transfer coefficient (α) of the diffusion controlled system by using Laviron's equation (eqn. b, 1980) as follows:[6]

$$E_{PA} = E_0 + (RT/\alpha nF)\left[\ln RT(K_s/\alpha nF) + \ln v\right]$$

Where, E_0, E_{PA}, T, R, F, n and v are the formal potential, anodic peak potential, temparature, gas constant, Faraday's constant, electron trnasfer number, and scan rate, respectively. Fig. S9 exhibits the linear calibration plot of E_{PA} with log of different sweep rates at fixed concentration of ChOH. From the slope of the plot, we have evaluated α and K_s and the values were found to be 0.37 and 13.34 s^{-1}.
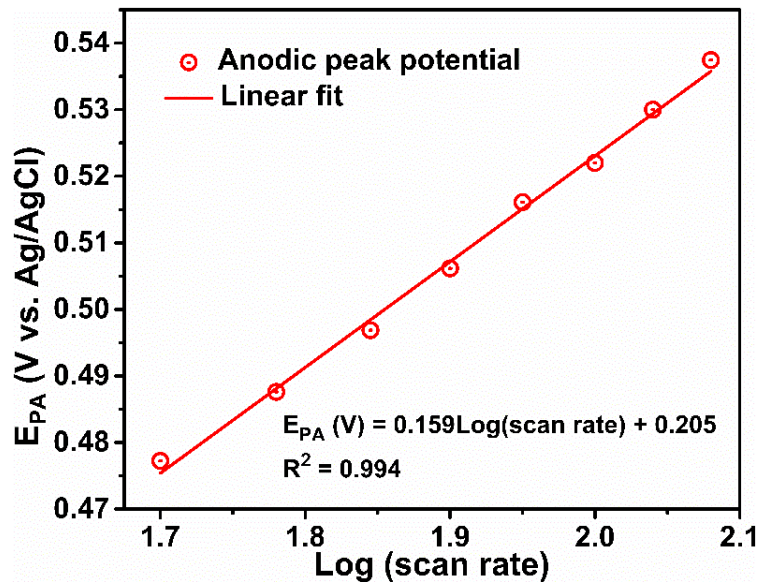

Fig. S9: Linear calibration plot of ZnO/WO_3 composite film using Laviron's equation of anodic peak current vs. log sweep rate.

Calculation of Electrochemical Active Surface Area

The electrochemical active surface area (ECSA) of all catalysts was calculated from the double-layer capacitance (C_{dl}) according to the following equation:[7]

$$ECSA = C_{dl}/C_s$$

Where C_s is the ideal specific capacitance of a smooth planar surface made of the same material per unit area under identical electrolyte conditions. The specific capacitance of the samples in the three-electrode system can be calculated from the CV curve using following equation:[8,9]

$$C_s = \frac{\overline{Q}}{m\Delta V}$$

Where, Q is the average charge during charging and discharging in coulomb, m is the mass of the active material in gram, ΔV is the potential window in volts.

Therefore, the C_s of the film can also be calculated from the charge-discharge of the CV curve as follows,

$$C_s = \frac{\overline{\int_{V1}^{V2} Ivdv}}{2\omega m\Delta V}$$

$\int_{V1}^{V2} Ivdv$ represents the absolute area of the charging-discharging CV curve in the potential window of V_1 to V_2, and ω is the scan rate of the voltammogram in volts per sec. In our case the mass of the deposited sample was 3mg for ZnO/FTO and WO$_3$/FTO and 4mg for WO$_3$/ZnO/FTO film. Therefore, C_s can be calculated from the slope ($2mC_s\Delta V$) of the linear plot of of absolute area vs. scan rate (Fig. S9).

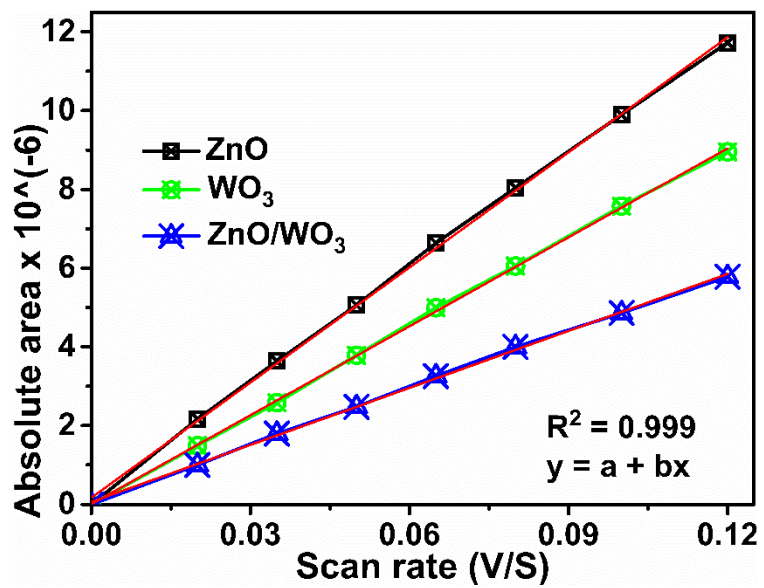**Fig. S10:** Linear plot of absolute area vs. scan rate of ZnO, WO_3 and ZnO/WO_3 thin films in
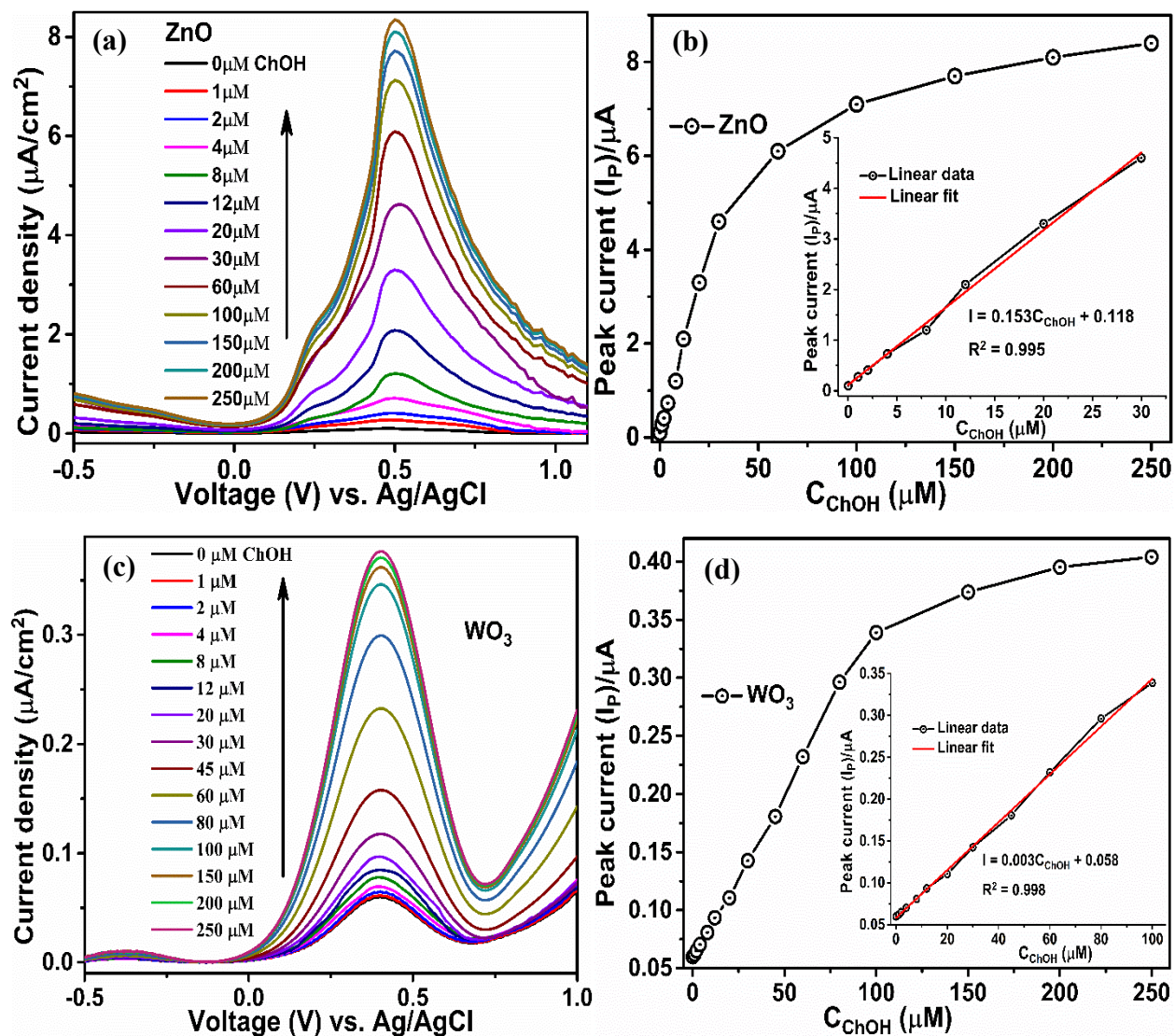
0.1(M) PBS (pH = 7.2).

Fig. S11: (a) and (c) are electrochemical DPV measurements of ZnO and WO$_3$ thin films with different concentrations of ChOH, (b) and (d) are peak current vs. concentration of Cholesterol calibration curves of corresponding films (inset is linear range of the calibration plots).
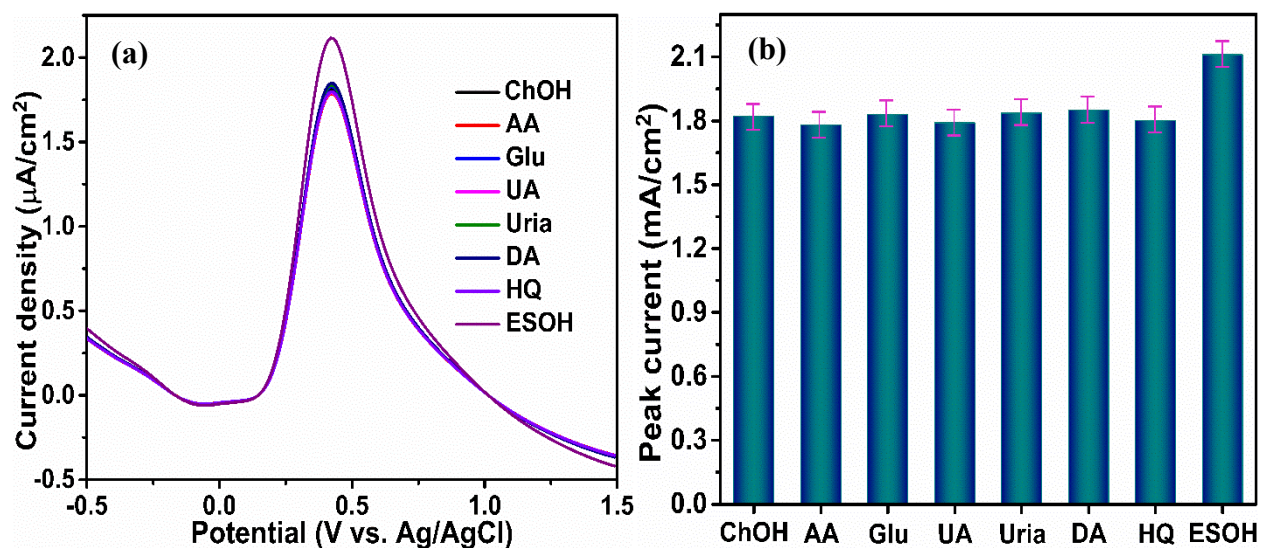
Fig. S12: (a) DPV measurements for selectivity test of ZnO/WO$_3$ layer-by-layer composite thin film in presence of Cholesterol (only 10μM) and for other anti-interfering compounds with 100μM conc. (b) corresponding bar diagram.
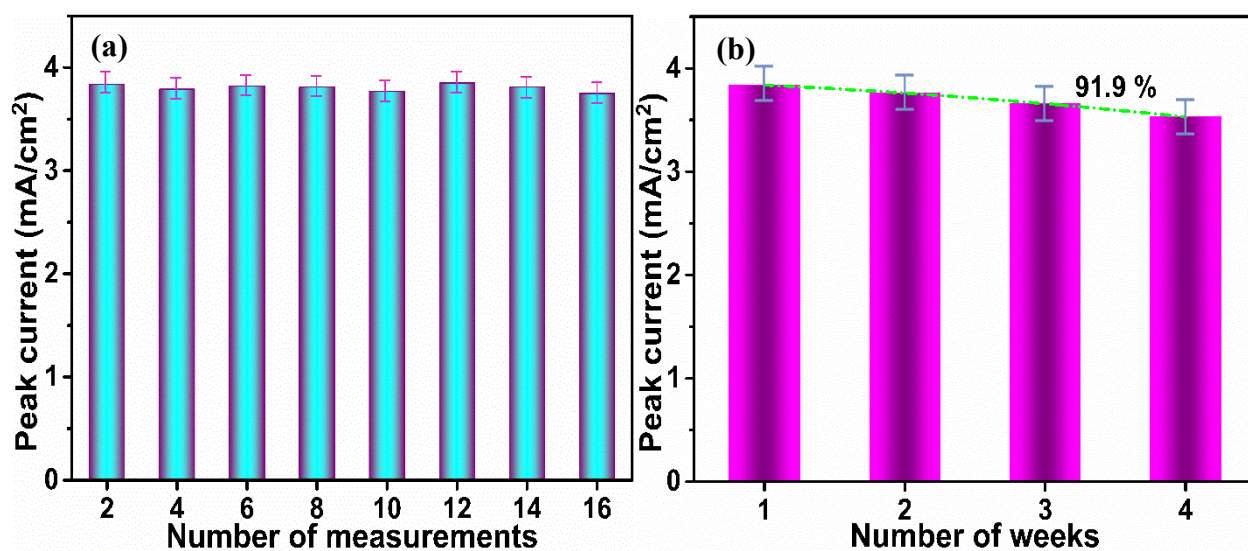

Fig. S13: (a) reproducibility test and (b) stability test of ZnO/WO$_3$ composite thin film in 0.1(M) PBS containing 60μM ChOH, respectively.
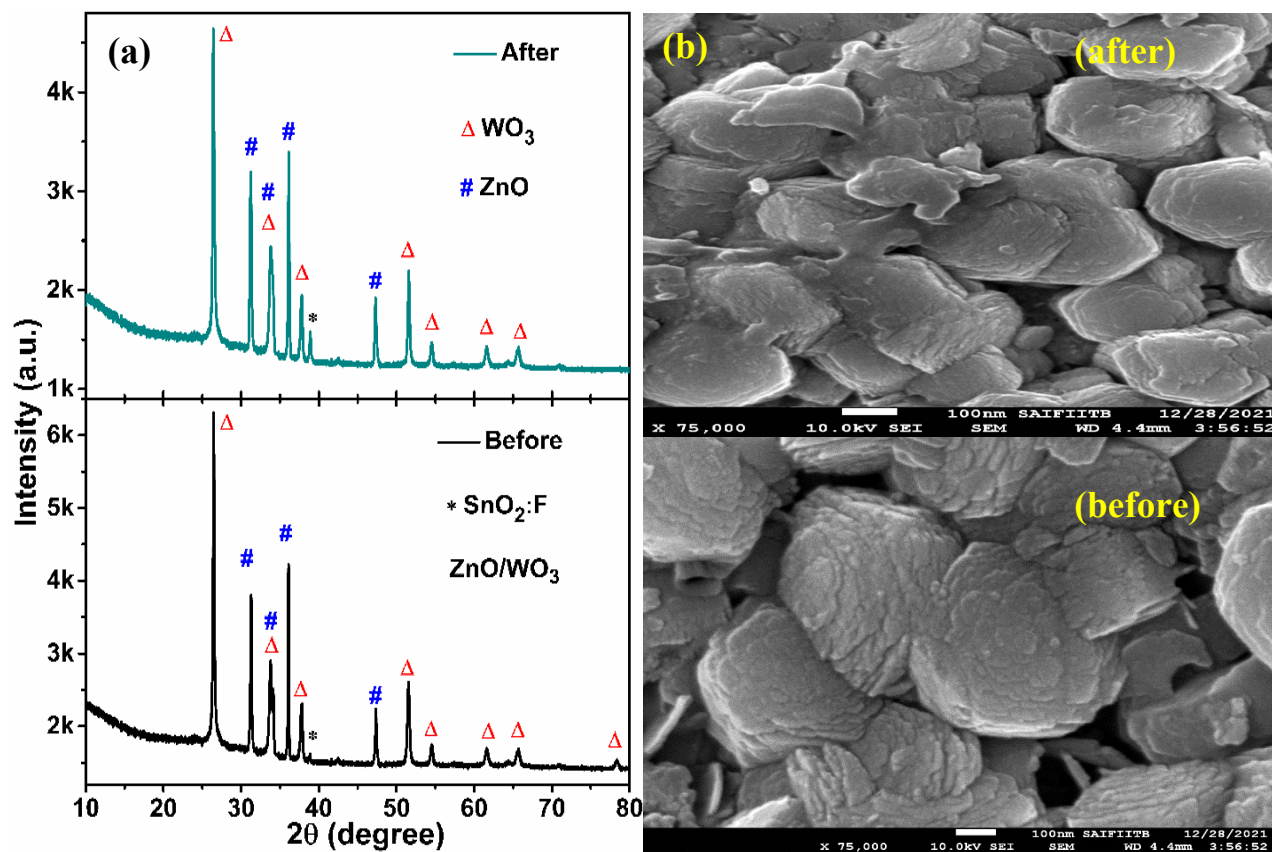
Fig. S14: (a) and (b) XRD and FESEM images of the ZnO/WO_3 composite thin film before and after the electro-oxidation of Cholesterol, respectively.

Table S2: Comparative study of the electrochemical non-enzymatic Cholesterol sensing

Sensors	Sensing Method	Electrode type	Electrolyte, pH	LOD (µM)	Linear range (µM)	Sensitivity (µA cm^{-2} mM^{-1})	Response time (s)	Reference
PANI/MWCNT s/starch	Cyclic voltammetry	Carbon paste	0.1m PBS, 5.0	10	32-5000	800	4-6	10
Cu$_2$O NPs/TNTs	Amperometry	Ti-foil	0.1M PBS, 7.0	0.05	24.4-6220	6034	3	11
Grp/β-CD/Methylene Blue	DPV	Sensing probe	0.1M PBS, 7.4	<1	1-100	0.01	~20	12
NiO/CVD grown graphene	Chronoamperometry	SiO$_2$/Si substrate	1M KOH, --	0.13	2-40	40.6	5	13
ZnO nanorods	Cyclic voltammetry	Si wafer microelectrode	0.02M PBS, 7.0	1780	1000-9000	4.2	---	14
Ag NPs-ZnO nanorods	Cyclic voltammetry	Si wafer microelectrode	0.02M PBS, 7.0	184	1000-9000	135	---	14
CuO: GNS composite	Colorimetric	----	0.02M PBS, --	78	100-800	-	---	15
PMO/Cu/Ni/C	DPV	Film	0.1M PBS, 7.0	0.051	40-6000	226.3	---	16
PMO-NiO/MoS$_2$/SPCE	DPV	Screen printed carbon electrode (SPCE)	0.1M PBS, 7.0	5.17	25.86-390	30.63	---	17
ZnO/WO$_3$/FTO	DPV	Thin Film	0.1M PBS, 7.2	0.0055	0-320	176.6	2	This Work

References

1   S. Goel, N. Sinha, H. Yadav, S. Godara, A. J. Joseph, B. Kumar, Ferroelectric Gd-doped ZnO nanostructures: Enhanced dielectric, ferroelectric and piezoelectric properties, *Mater. Chem. Phys.,* 2017, **202,** 56-64.

2   Md. M. Obeid, H. R. Jappor, K.Al-Marzoki, I. A. Al-Hydary, S. J. Edrees, M. M. Shukur, Unraveling the effect of Gd doping on the structural, optical, and magnetic properties of ZnO based diluted magnetic semiconductor nanorods, *RSC Adv.,* 2019, **9,** 33207-33221.

3   S. Pokhrel, J. Birkenstock, A. Dianat, J. Zimmermann, M. Schowalter, A. Rosenauer, L. Colombi Ciacchi, L. Mädler, In situ high temperature X-ray diffraction, transmission electron microscopy and theoretical modeling for the formation of WO_3 crystallites, *CrystEngComm.,* 2015, **17,** 6985-6998.

4   M. Gaudon, O. Toulemonde, A. Demourgues, Green Coloration of Co-Doped ZnO Explained from Structural Refinement and Bond Considerations, *Inorg. Chem.,* 2007, **46,** 10996-11002.

5   J. J. Beltra´n, C. A. Barrero, A. Punnoose, Understanding the role of iron in the magnetism of Fe doped ZnO nanoparticles, Phys. Chem. Chem. Phys. 17 (2015) 15284-15296.

6   A. J. Bard, L. R. Faulkner, Electrochemical methods: fundamentals and applications, *Wiley*, New York, **1980**.

7   U. K. Ghorui, P. Mondal, B. Adhikary, A. Mondal, A. Sarkar, Newly Designed One-Pot In-Situ Synthesis of VS_2/rGO Nanocomposite to Explore Its Electrochemical Behavior towards Oxygen Electrode Reactions, *ChemElectroChem,* 2022, **9,** e202200526.

8   J. Yu, N. Fu, J. Zhao, R. Liu, F. Li, Y. Du, Z. Yang, High Specific Capacitance Electrode Material for Supercapacitors Based on Resin-Derived Nitrogen-Doped Porous Carbons, *ACS Omega,* 2019, **4**, 15904−15911.

9   M. Sethi, U. S. Shenoy, D. K. Bhat, A porous graphene–$NiFe_2O_4$ nanocomposite with high electrochemical performance and high cycling stability for energy storage applications, *Nanoscale Adv.*, 2020, **2**, 4229–4241.

10   V. Gautam, K. P. Singh, V. L. Yadav, Polyaniline/MWCNTs/starch modified carbon paste electrode for non-enzymatic detection of cholesterol: application to real sample (cow milk), *Analytical and Bioanalytical Chemistry*, 2018, **410**, 2173–2181.

11   N. Khaliq, M. A. Rasheed, G. Cha, M. Khan, S. Karim, P. Schmuki, Development of non-enzymatic cholesterol bio-sensor based on TiO2 nanotubes decorated with Cu2O nanoparticles, *Sensors and Actuators, B: Chemical*, 2020, **302**, 127200.

12   N. Agnihotri, A. D. Chowdhury, A. De, Non-enzymatic electrochemical detection of cholesterol using β-cyclodextrin functionalized graphene, *Biosensors and Bioelectronics,* 2015, **63,** 212–217.

13   A. Rengaraj, Y. Haldorai, C. H. Kwak, S. Ahn, K. J. Jeon, S. H. Park, Electrodeposition of flower-like nickel oxide on CVD-grown graphene to develop an electrochemical non-enzymatic biosensor, *Journal of Materials Chemistry B*, 2015, **3,** 6301–6309.

14   T. T. N. Anh, H. Lan, L. T. Tam, V. H. Pham, P. D. Tam, Highly sensitive nonenzymatic cholesterol sensor based on zinc oxide nanorods, *Journal of Electronic Materials*, 2018, **47,** 6701–6708.

15   V. Sharma, S. M. Mobin, Cytocompatible peroxidase mimic CuO:graphene nanosphere composite as colorimetric dual sensor for hydrogen peroxide and cholesterol with its logic gate implementation, *Sensors and Actuators, B: Chemical*, 2017, **240,** 338–348.

16   P. K. Bairagia, N. Vermaa, Electrochemically deposited dendritic poly (methyl orange) nanofilm on metal-carbon-polymer nanocomposite: A novel non-enzymatic electrochemical biosensor for cholesterol, *Journal of Electroanalytical Chemistry,* 2018, **814,** 134–143.

17   H. A. Ariyanta, T. A. Ivandini, Y. Yulizar, Poly (methyl orange)-modified NiO/MoS2/SPCE for a non-enzymatic detection of cholesterol, *FlatChem,* 2021, **29,** 100285.